Met O (APR) Turbulence and Diffusion Note No. 265

Momentum balance over one wavelength of a series of hills: modelling aspects and comparison with wind tunnel measurements

by

M. Athanassiadou

22 February 2000

Met O (APR)
(Atmospheric Processes Research)
Meteorological Office
London Road
Bracknell
Berks, RG12 2SZ

Note

This paper has not been published. Permission to quote from it should be obtained from the Assistant Director, Atmospheric Processes Research Division, Met O (APR), Meteorological Office, London Road, Bracknell, Berkshire, RG12 2SZ.

Momentum balance over one wavelength of a series of hills: modelling aspects and comparison with wind tunnel measurements

Maria Athanassiadou

22 February, 2000

Abstract

In this note, the momentum balance over one wavelength of a series of hills is discussed. Results are obtained from different types of numerical simulations and compared with available data from wind tunnel measurements. Intercomparisons between model runs are also made, with emphasis on the best way to compare numerical simulations with observations. Some basic flow characteristics from the simulations are also discussed and compared with the observations. The flow characteristics include the basic structure of the boundary layer over flat terrain as well as over a series of small and large hills (maximum slope of 0.2 and 0.4 respectively). In the case of the large hills, flow separation is observed in both the observations and the numerical results.

1 Introduction

Hills with maximum height of a few hundred meters and horizontal dimensions of a few kilometers, cannot be explicitly resolved in numerical weather prediction models with their horizontal resolutions of 10 km or more. Nevertheless, their impact on the flow is significant and their effects need to be parametrised. The work of Newley (1985) and Wood and Mason (1993), amongst others, has shown the existence of a drag force for neutral flow over hills, due to the pressure being out of phase with the hill. The total surface drag over hilly terrain is therefore enhanced compared with that over flat terrain of the same roughness cover. Despite the considerable progress made over the last years in better representation of complex terrain processes, there is still only limited confidence in our ability to predict such quantities as the total drag over hilly terrain.

Analytical work is based on linear analysis, and hence hindered by its limitations i.e., small slopes, no separation. The main tool of investigation tends to be numerical modelling, although a number of studies have shown sensitivity to the turbulence model used. For example, a mixing length model (as used in the present study) tends to overestimate stress perturbations in the Jackson and Hunt (1975) outer region, often leading to an overprediction of the pressure drag (Wood and Mason 1993). However, even with a mixing length model, further issues arise relating to the most appropriate way to set up the model in order to make direct comparisons with observational data.

In this note, direct comparisons are made between numerical simulations and physical modelling measurements, with the objective to clarify issues relating to the most appropriate and acceptable way to simulate flow over an infinite series of hills. The balance of terms in the momentum budget is discussed. The observations consist of wind tunnel measurements of the mean flow, turbulence statistics and surface pressure over a series of rough sinusoidal hills and were made in the EnFlo Laboratory, at the University of Surrey. The numerical simulations are mixing length runs and were performed using the numerical model BLASIUS.

2 Mathematical Representation

The steady state, 2D momentum equation in the x - direction can be written as:

$$\frac{\partial(UW)}{\partial z} + \frac{\partial U^2}{\partial x} = -\frac{\partial P_i}{\partial x} - \frac{\partial P}{\partial x} + \frac{\partial \tau_{13}}{\partial z} + \frac{\partial \tau_{11}}{\partial x} \tag{1}$$

(I) (II) (III) (IV) (V) (VI)

where U and W are the ensemble mean velocities in the x and z directions respectively. Term (III) refers to any imposed pressure gradient used to drive the flow and Term (IV) to any pressure gradient developed by the model.

We integrate equation (1) over one wavelength (λ), in the horizontal and from the surface $z = z_s(x)$ to the top of the domain H. We make use of the following formula:

$$\int_{-\lambda/2}^{\lambda/2}\int_{z_s}^{H} \frac{\partial f}{\partial x} dz dx = \int_{-\lambda/2}^{\lambda/2} \frac{\partial}{\partial x} \int_{z_s}^{H} f dz dx + \int_{-\lambda/2}^{\lambda/2} f_s \frac{\partial z_s}{\partial x} dx \tag{2}$$

where f is any parameter in equation (1). Then the individual terms in equation (1) can be written as follows.

$$(I) \Rightarrow \qquad \int_{-\lambda/2}^{\lambda/2}\int_{z_s}^{H} (I) = 0 \tag{3}$$

because of the boundary conditions (B.C.s), (vertical velocity is zero at the top and bottom of the domain).

$$(II) \Rightarrow \qquad \int_{z_s}^{H} U^2|_{-\lambda/2}^{\lambda/2} dz = \int_{z_s}^{H} U_{\lambda/2}^2 dz - \int_{z_s}^{H} U_{-\lambda/2}^2 dz. \tag{4}$$

$$(III) \Rightarrow \qquad -C_{ipg} \int_{-\lambda/2}^{\lambda/2}\int_{z_s}^{H} dz\, dx = -C_{ipg} \int_{-\lambda/2}^{\lambda/2} (H - z_s) dx = -C_{ipg}\,(H - h/2)\,\lambda \tag{5}$$

where $C_{ipg} = \partial P_i/\partial x$ is the imposed pressure gradient that drives the flow in certain cases (and it is constant in space and time). h is the maximum height of the topography whose profile is defined in the next section.

$$(IV) \Rightarrow \qquad -\left[\int_{z_s}^{H} P_{\lambda/2}\, dz - \int_{z_s}^{H} P_{-\lambda/2}\, dz\right] - \int_{-\lambda/2}^{\lambda/2} p_s \frac{\partial z_s}{\partial x}\, dx \tag{6}$$

$$(V) \Rightarrow \qquad \int_{-\lambda/2}^{\lambda/2} (\tau_{13}(H) - \tau_{13}(z_s))\, dx = -\int_{-\lambda/2}^{\lambda/2} \tau_{13}(z_s) dx \tag{7}$$

because of the B.C.s (stress is zero at the top of the domain).

$$(VI) \Rightarrow \qquad \left[\int_{z_s}^{H} \tau_{11\lambda/2}\, dz - \int_{z_s}^{H} \tau_{11-\lambda/2}\, dz\right] + \int_{-\lambda/2}^{\lambda/2} \tau_{11s} \frac{\partial z_s}{\partial x}\, dx \tag{8}$$

Defining, for convenience, the operator:

$$\Delta[\,.\,] = \frac{1}{\lambda}\left[\int_{z_s}^{H} [\,.\,]_{\lambda/2}\, dz - \int_{z_s}^{H} [\,.\,]_{-\lambda/2}\, dz\right] \tag{9}$$

we write the balance of terms in (1) in a concise way, after dividing all terms by λ, as follows:

$$\begin{aligned} \Delta[U^2] &= -C_{ipg}\,(H - h/2) - \Delta[P] - F_p - u_\star^2 + \Delta[\tau_{11}] \\ \text{MF} &= +\,\text{IG} + \text{PR} + \text{SP} + \text{SS} + \text{SR} \end{aligned} \tag{10}$$

where,

MF: streamwise momentum flux difference across a wavelength

IG: imposed pressure gradient term (certain cases)

PR: model pressure drop

SP: surface pressure drag

SS: surface stress (shear stress and non isotropic normal stress)

SR: streamwise stress difference across a wavelength

In a simulation where open B.C.s are employed, the imposed pressure gradient term IG, is usually set to zero. What happens when this is not the case, is discussed later in the next section. In a simulation with periodic B.C.s, the Δ terms are identically zero and so, the imposed pressure gradient balances the surface pressure drag and surface stress i.e., IG = SP + SS.

3 Simulations

It is not always clear how best to perform a simulation to compare with observational data. The wind tunnel configuration of 12 hills aims at reproducing neutral flow over an infinite series of hills. When doing the same thing with the model, the obvious thing that springs into mind is to have one wavelength with periodic boundary conditions. In this case, the model requires that we specify a domain height and a way to drive the flow. In the absence of Coriolis force, as in the present case, and for *periodic boundary conditions* in the x - direction, we have two options:

- No pressure gradient is imposed in the streamwise direction and the flow is driven by a specified velocity at the top U_{top}. The boundary layer grows in time (which is equivalent to a wind tunnel

one growing with downstream distance), eventually producing non-zero stress at the domain top which is not a realistic condition in our case.

- A specified pressure gradient is imposed in the streamwise direction and a stress free upper boundary condition is used. This choice produces an equilibrium boundary layer with depth equal to the domain height and a linear stress profile with height that goes to zero at the top. As a result, ad hoc knowledge (or a good estimate) of the boundary layer depth is required. This is a more appropriate choice for the present case (although it could not be used in a case of stable stratification with gravity waves for example, where we do not want turbulent fluxes at the upper part of the domain).

The other possible thing to do is to use open B.C.s and impose an inflow wind profile, with the domain in the numerical simulations as close to the wind tunnel configuration as possible. In this case, we do not impose any pressure gradient in the streamwise direction. Even if we do, it would make no difference since the model will develop a 'counter pressure gradient' in this case. The change in the PR term exactly balances the change in the IG term,while the other terms remain unchanged. Simulations have been performed to test and verify this argument. The balance of terms from such a simulation is included in Table (2) in the next section, along with the main results.

In the case of *open boundary conditions*, we again have a choice of two top B.C.s:

- We can impose a constant velocity at the top boundary. As the flow near the surface has to slow down, because of mass conservation, there must be a region where the velocity is greater than the inflow velocity. This type of speed up occurs just above the boundary layer. Above that height, $dU/dz < 0$ in order to get back to the fixed U_{top} boundary condition. This results in the stress being negative in that region. Such a stress profile does not conform with the structure of the boundary layer from the observations.
- The second choice is to impose a zero stress top boundary condition. Preliminary tests with this option made it clear that this is the best overall choice, especially with the top boundary sufficiently far away so as not to influence the solution.

The simulations aim at reproducing the flow over the series of hills in the experiments. Although some comparisons are made of the mean flow and turbulence from the model runs and experimental data, the main objective is to perform a momentum balance over one wavelength for both the small and large hill cases. The momentum balance is not obtainable from the wind tunnel measurements explicitly. However, it can be obtained from BLASIUS runs, since all terms in (10) are given explicitly from the model. General comparison of the flow between the measurements and BLASIUS runs aim to make sure that the latter are realistic simulations of the former so that the momentum balance results can be believed to hold in general. The dimensions of the domain used in the open boundary conditions numerical simulations ($4.62 \times 0.9 \times 0.6$ m in the (x,y,z) directions respectively) are the same as those of the wind tunnel. The grid spacing is 16.5 mm in the horizontal with a variable spacing grid in the vertical varying from 2.05 mm near the surface to 6.46 mm aloft. All runs use a first order mixing length closure with a length scale $L_0 = 30$ mm. This value is of order of 1/3 of the boundary layer depth.

The first simulation is of neutral flow over a flat surface using the full domain and open B.C.s in the streamwise direction. This was done in order to make sure that the model can reproduce a realistic boundary layer over flat terrain before the hills were introduced. It also serves for comparisons with the boundary layer, to be examined later, over the hills. The numerical model was initialised with constant wind and neutral temperature profiles. The roughness length z_o is set to 0.337 mm, the same as the value obtained from the experimental data, a zero stress condition is imposed at the top boundary and there is no imposed pressure gradient across the domain.

The second case consists of 12 small hills with open B.C.s. The basic setup of the flow is the same as in the flat run. The only difference is in the topography (lower boundary) of the model. In this case, there are 12 hills. A flat surface equal in length to the wavelength of one hill is used in front of the first hill to reduce the impact on the impinging flow. A similar flat surface is used at the end of the domain after the 12th hill. The total domain length remains the same as before.

The third case involves one small hill in a periodic domain with the domain length equal to one hill length. The domain depth H, is set equal to the boundary layer depth obtained over the 10th hill from the open B.C. run. The imposed pressure gradient C_{ipg}, for the periodic B.C. run is then set through

$$C_{ipg}[H - h/2] = F_p + u_*^2 \qquad \Rightarrow \qquad C_{ipg} = (F_p + u_*^2)/[H - h/2] \tag{11}$$

Here F_p and u_*^2 are the values obtained from the open B.C. run, over the 10th hill. This procedure ensures that the sum of the surface stress and pressure drag is the same as in the open B.C. simulation. The advantage of this type of simulation, if it can be shown to produce acceptable results, is that it is much cheaper computationally than the one which simulates flow over 12 hills. When using a more expensive modelling technique e.g. Large Eddy Simulation, it might be the only approach that is feasible.

The fourth and fifth cases investigate the flow over the large hills in a similar configuration to the second and third cases. The cases are summarised in Table (1). An extra simulation (R033), shown in Table (1), examines the effect of using open B.C.s and imposing a pressure gradient in the streamwise direction at the same time.

Table 1: Description of simulations

	Case description	*Run number*
CASE 1:	Flat roughness - open B.C.s, IG = 0	R023
CASE 2:	12 small hills - open B.C.s, IG = 0	R024
CASE 3:	1 small hill - periodic B.C.s, IG $\neq$ 0	R025
CASE 4:	12 large hills - open B.C.s, IG = 0	R026
CASE 5:	1 large hill - periodic B.C.s, IG $\neq$ 0	R027
CASE 6:	Flat roughness - open B.C.s, IG $\neq$ 0	R033

In all hilly runs, the hill profile is given by:

$$z_s(x) = h\, cos^2\,(\pi x/\lambda) \tag{12}$$

where h is the maximum height of the hill and λ is the wavelength.

4 Results

The development of streamwise velocity in the flat case is shown in Fig. (1). The boundary layer depth at 3.5 m downstream is about 100 mm. This is diagnosed as the height at which the shear stress has a value equal to 5% its surface value. The downstream position of 3.5 m is the location of the 10th hill and also close to the positions where measurements were taken over the flat surface in the wind tunnel. The friction velocity at the same downstream position is 0.6 m/s. Vertical profiles of the mean velocity and shear stress, Fig. (2), at that position show excellent agreement with the wind tunnel data.

Fig. (3)(a)-(b) show the shear stress over the small and large hills respectively. The contour interval for the large hills is twice that for the small hills. In both cases we see the boundary layer growing with downstream distance. At x = 3.5 m, the boundary layer depth is about 165 mm and 210 mm over

the small and large hills respectively. These values were used as domain heights for the one wavelength simulations of small and large hills. The boundary layer depth is obtained from the shear stress profile over the 10th hill in the same way as for the flat surface.

Fig. (4) shows the flow between the 9th and 10th large hills. Solid contours represent positive horizontal velocity and dashed ones negative horizontal velocity. Flow separation can be seen to have occurred in the simulation. The flow detaches at about -100 mm from the trough and reattaches at about 50 mm downstream of the trough. These values compare very well with the wind tunnel observations.

Comparisons between the two types of simulations are shown in Fig. (5) and Fig. (6) for the small and large hills respectively. The figures show the mean wind and shear stress over the 10th hill from the open B.C.s simulations and over the one hill from the simulations with periodic boundary conditions. The fields from the two types of simulations are virtually indistinguishable, for both the small and large hills. The contour interval is the same for all cases, 0.5 m/s for the mean velocity and 0.1 m^2/s^2 for the shear stress.

Table 2: Balance of terms in equation (10).

	MF	IG	PR	SP	SS	SR	residual
CASE 1	0.1419	0	0.5201	N/A	-0.3956	4.8×10^{-5}	0.0174
CASE 2	0.2169	0	0.7247	-0.1726	-0.3370	0.00039	0.0015
CASE 3	0	0.5100	0	-0.1625	-0.3497	0.	0.0022
CASE 4	0.3258	0	1.1140	-0.5776	-0.2094	0.00136	-0.0026
CASE 5	0	0.7860	0	-0.5598	-0.2337	0.	0.0075
CASE 6	0.1419	1.9800	-1.4612	N/A	-0.3956	4.8×10^{-5}	0.0187

The surface pressure distribution on the hills is now considered. It is important to get it right because it relates to the surface pressure drag induced by the hill. Fig (7)(a)-(b) show the distribution of the surface pressure p_s (normalised by $0.5\rho U_r^2$, where U_r is the free stream velocity) over the small and large hills respectively. Results obtained from the one wavelength simulations with periodic B.C.s are shown as solid lines. The pressure distributions over the 10th hill from the 12 hills simulations using open B.C.s are shown as dashed lines. Wind tunnel measurements are shown in asterisks. There is a constant shift in the pressure between the simulations with open B.C.s and periodic ones that does not affect the surface pressure drag, as is shown in Table (2), since the pressure in the model is arbitrary within an additive constant. The shape of the normalised pressure from the measurements is a bit different from that of the numerical simulations but again the surface pressure drag from the measurements compares rather well with that from the numerical simulations as shown in Table (3).

All of the terms in the momentum budgets of the six cases are shown in Table (2). Note that the residuals are small in all cases. However, the residuals for the hill cases are an order of magnitude smaller than the ones for the roughness only cases. The reason for that is not clear. In the open B.C. runs (when IG = 0), the model develops its own pressure gradient. Table (2) also confirms that as previously mentioned, addition of an imposed pressure gradient in open B.C. runs (case 6 vs case 1), causes only an equal and opposite change to the model developed pressure gradient, so that the other terms in the budget remain unchanged.

The sum of the magnitudes of the surface pressure drag and surface friction can be seen as an effective surface stress for the flow aloft. Normalising by the free stream velocity, the above statement can be expressed as:

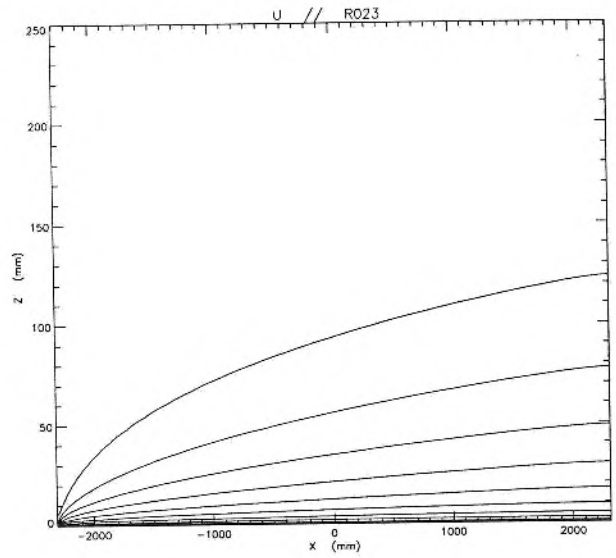

Figure 1: Mean streamwise velocity over the flat surface. The contour interval is 1 m/s. The top contour corresponds to 10 m/s.

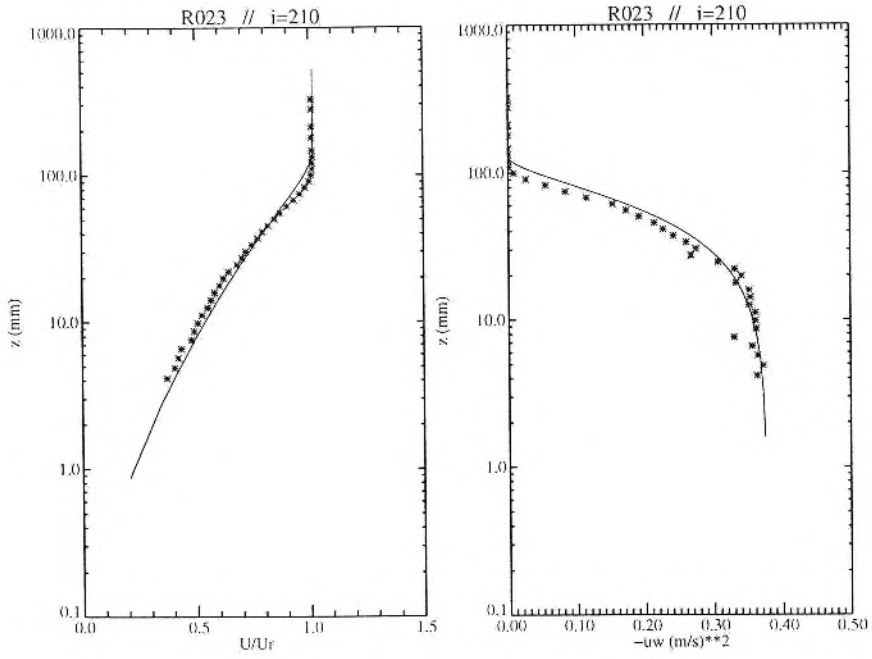

Figure 2: Profiles over the flat surface at a distance about 3.5 m downstream, shown in solid lines. Measurements are shown in asterisks (a) Mean velocity, (b) Shear stress

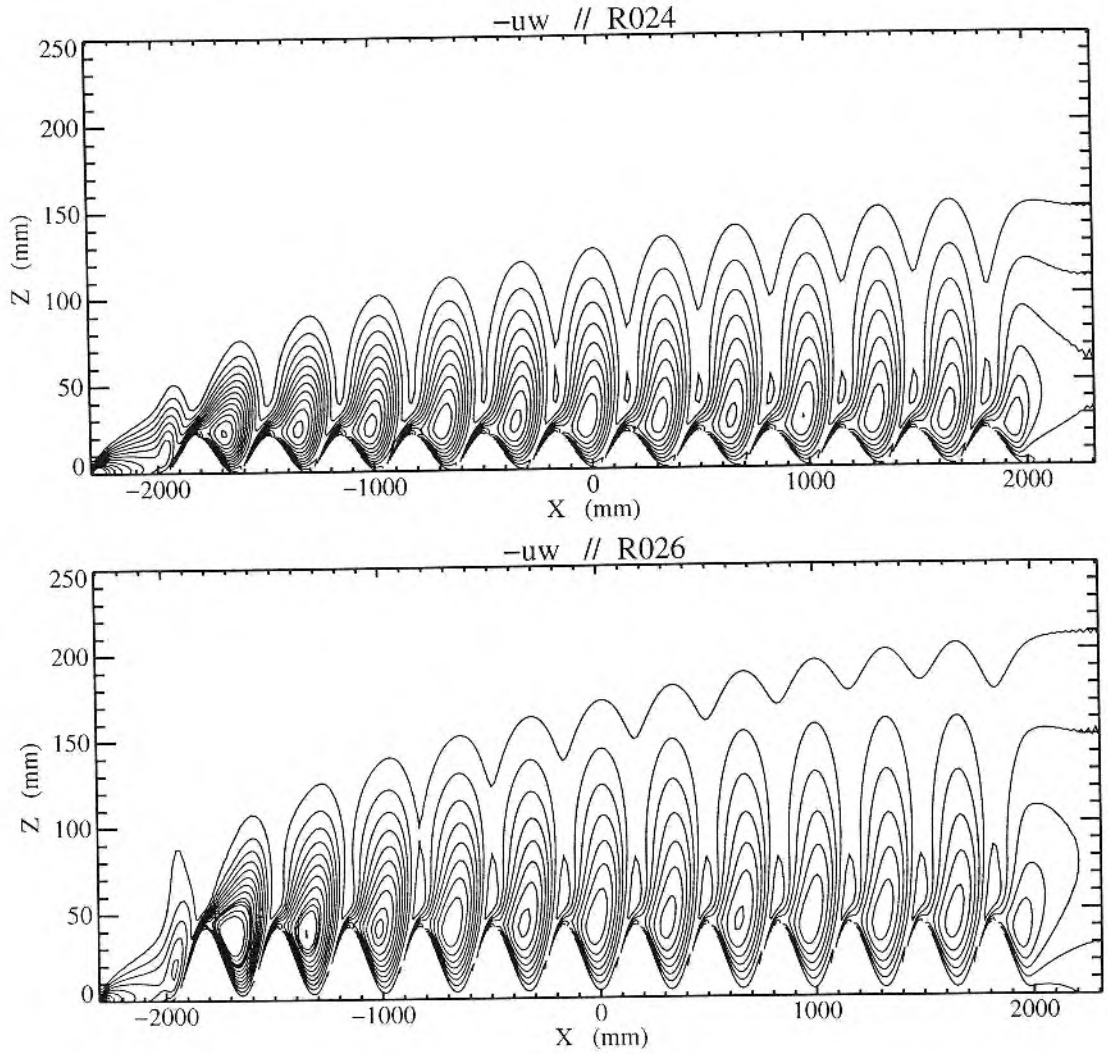

Figure 3: Shear stress over (a) the small hills, (b) the large hills

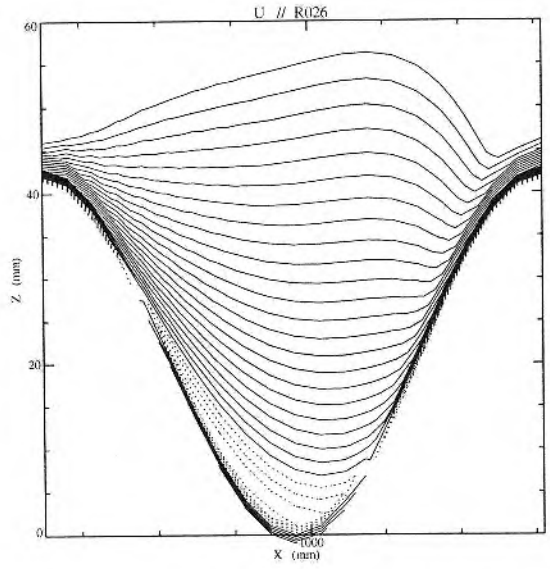

Figure 4: Streamwise velocity between the 9th and 10th hills. Solid contours for positive U, dash for negative U.

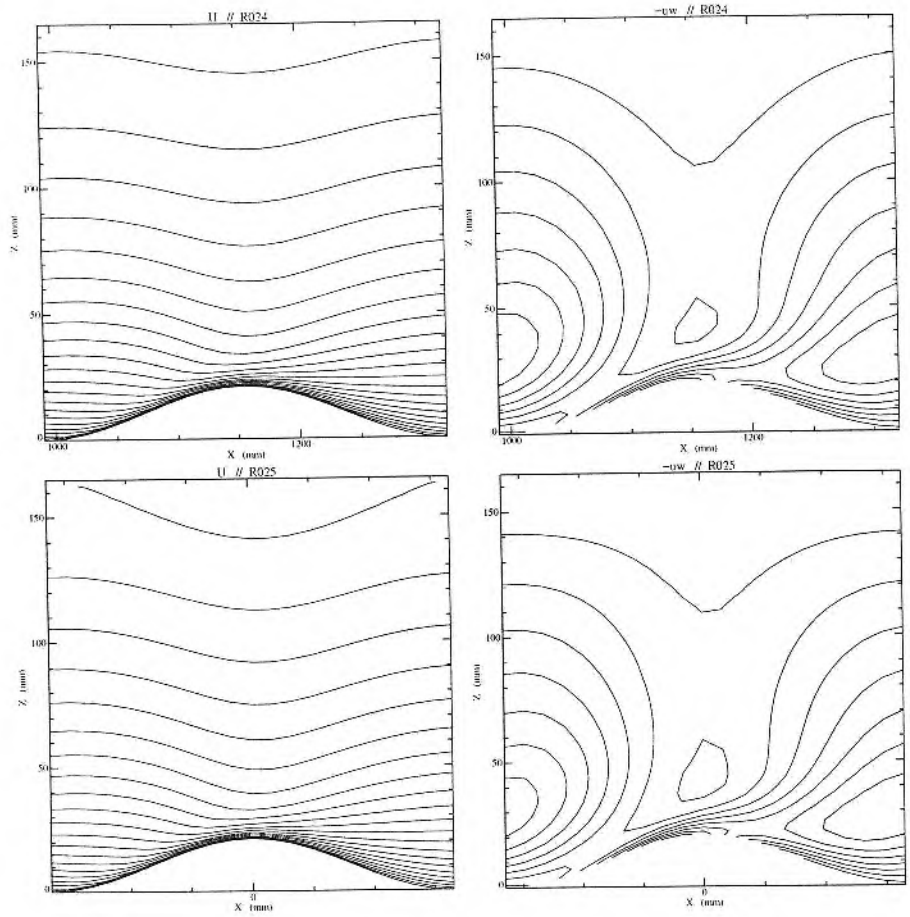

Figure 5: Comparison between simulations over the small hills. (a) U over the 10th hill, (b) -uw over the 10th hill, (c) U over the hill in periodic domain, (d) -uw over the hill in periodic domain

$$\left(\frac{u_*^{eff}}{U_r}\right)^2 = \frac{F_p}{\rho U_r^2} + \left(\frac{u_*}{U_r}\right)^2 \tag{13}$$

The relative magnitudes of terms in equation (13) are summarised in Table (3). Recall that the boundary layer depth and the imposed pressure gradient in the periodic B.C. simulations were chosen so that the sum of the surface stress and the pressure drag has to be the same as in the corresponding open B.C. simulations, and so the values of u_*^{eff}/U_r from cases 2 and 3 and from cases 4 and 5 are consistent. The partition into surface stress and pressure drag can also be seen to be robust, with similar values of u_*/u_*^{eff} obtained with the open and periodic B.C. runs (~ 0.67 for the small hills; ~ 0.28 for the large hills).

Table (3) also shows the equivalent results from the measurements. The total stress in the measurements is obtained by extrapolating the area averaged stress profile to the surface. It is therefore an estimation. The surface stress is the residual from the total stress and the surface pressure drag, the latter being the only one measured directly in the wind tunnel. The measurements and the numerical simulations agree rather well. The difference in the total stress between measurements and simulations is about 6% and 3% for the small and large hills respectively. The partitioning though of the total stress into pressure and friction drag is less accurate for the large hills than for the small hills.

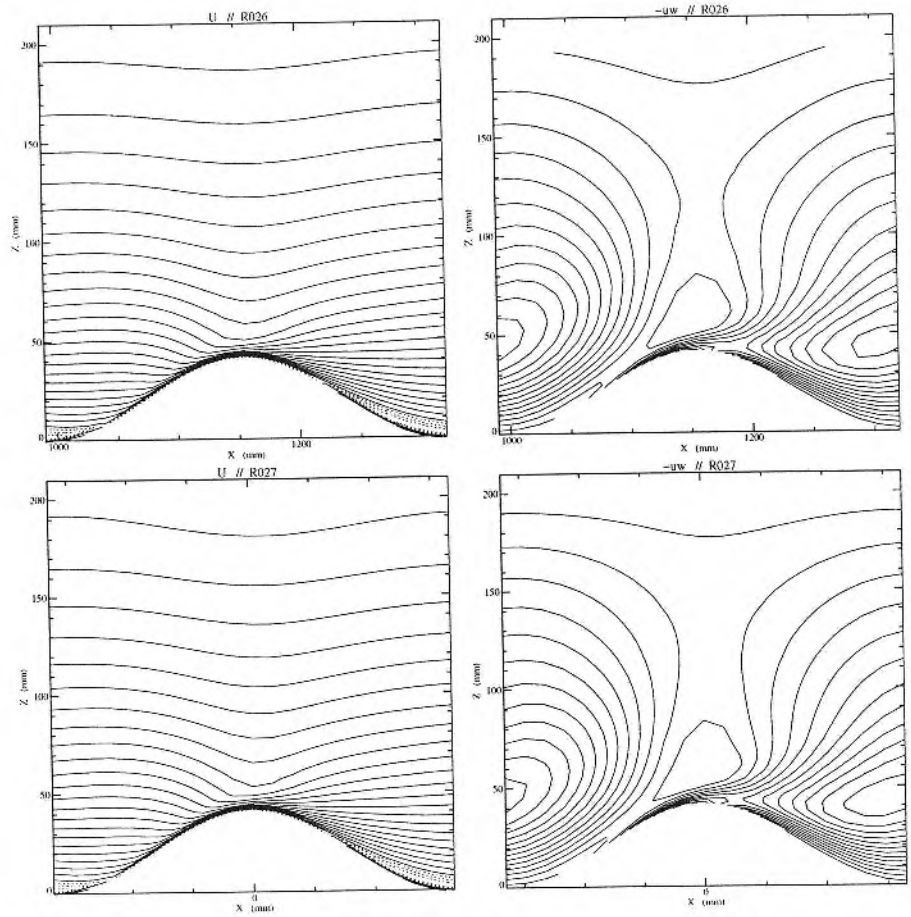

Figure 6: Comparison between simulations over the large hills. (a) U over the 10th hill, (b) -uw over the 10th hill, (c) U over the hill in periodic domain, (d) -uw over the hill in periodic domain

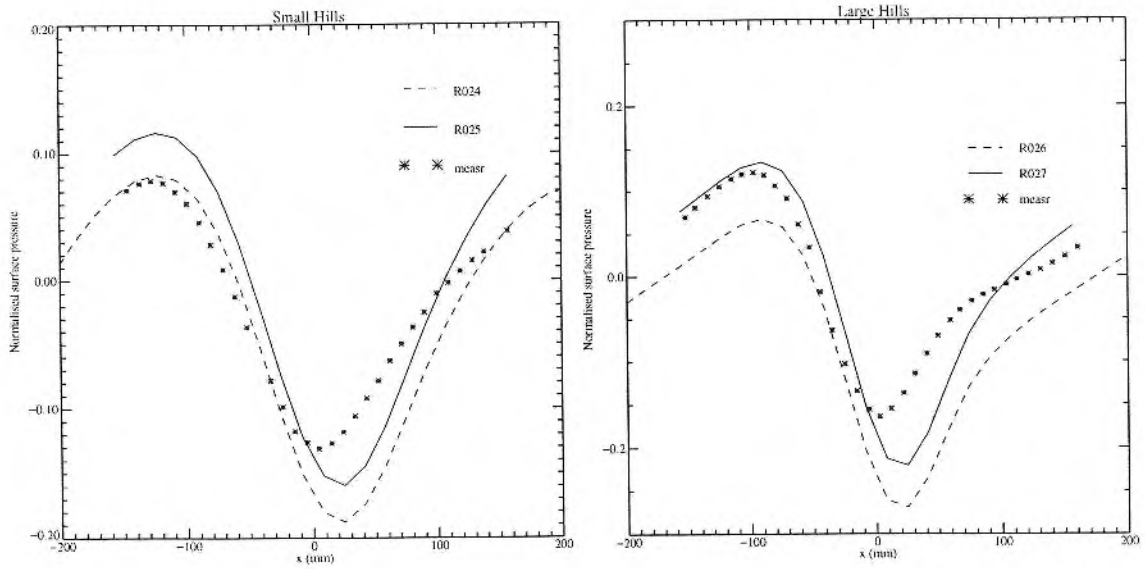

Figure 7: Normalised surface pressure ($p'/0.5\rho U_r^2$) over one wavelength. Solid lines are from the periodic domain simulations. Dashed lines over the 10th hill from the open boundary simulations. Asterisks are the wind - tunnel measurements over the 10th hill. (a) small hills, (b) large hills

Table 3: Relative magnitude of terms in (13)

	$(u_*^{eff}/U_r)^2 \times 10^3$	$F_p/\rho U_r^2 \times 10^3$	$(u_*/U_r)^2 \times 10^3$	u_*/u_*^{eff}	C
small hills measr	4.761	1.775	2.986	0.627	12
CASE 2	5.100	1.726	3.370	0.661	13
CASE 3	5.100	1.625	3.497	0.682	12
large hills measr	7.600	6.285	1.284	0.169	11
CASE 4	7.860	5.776	2.094	0.266	9
CASE 5	7.860	5.598	2.337	0.297	9

Another parameter shown is the drag coefficient for each case, given by

$$C = F_p/(u_{*o}^2 \sigma^2) \tag{14}$$

where σ is the slope of the hill and u_{*o} is the surface friction over a flat surface with the same roughness as the hills. Numerical studies (Newley 1985, Wood and Mason 1993), have concluded that a mixing length model overestimates the drag coefficient (typically, $C \sim 12$), compared to a second order closure model ($C \sim 6$). The results obtained from the measurements are closer to the typical values of a mixing length and almost double the second order closure model. This is at first surprising, although Wood and Mason (1993) showed that the drag coefficient increases as λ/z_o decreases. As a result, the discrepancy is not as large as it first appears.

5 Conclusions

In this note, the momentum budget over one wavelength in a series of hills has been examined for the case of neutral flow. Different ways to run a numerical model to simulate flow over an infinite series of hills were also discussed. Model results were compared with measurements taken over a series of hills in a wind tunnel under neutral stratification. The main conclusions are summarised below:

- Simulations with open B.C.s that mimic the wind tunnel configuration of 12 hills, produce results broadly consistent with the measurements taken in the wind tunnel. This is also the case for flow over a flat rough surface.
- Simulations with open B.C.s and 12 hills, produce very similar results (in terms of the partition into surface stress and pressure drag) to simulations with periodic B.C.s and one hill. This is the case over the 10th hill or in other words, sufficiently downstream for the boundary layer to have almost fully adjusted over the hills. Significant differences between the two approaches would be observed over the first or second hills.
- From a modelling point of view, when flow over an infinite series of hills is examined, the results in this note show that it is quite acceptable to use a periodic domain and one hill as opposed to a full domain with open B.C.s and many hills, since almost indistinguishable results are produced. This can be of particular importance in LES studies of flow over hills [2] where use of a full domain would be computationally impossible. One caution should be borne in mind. Although in the simulations with open B.C.s the value of the imposed pressure gradient does not matter i.e., it does not affect F_p or u_*, this is not the case in the simulations with periodic B.C.s imposed in the streamwise

direction. In the latter case, both the imposed pressure gradient and the depth of the domain, being in effect the boundary layer depth, influence the results and care should be taken to choose appropriate values. This is particularly important when direct comparisons with observations are sought.

Acknowledgements

The author wishes to thank Nigel Wood and Andy Brown for their helpful comments at various stages of this work.

References

[1] Athanassiadou M. and I.P. Castro, 1999: 'The flow over rough sinusoidal hills'. Report ME-FD / 99.99, EnFlo, University of Surrey.

[2] Brown A., J.M. Hobson and N. Wood, 2000: 'Large eddy simulations of neutral turbulent flow over rough sinusoidal ridges'. Submitted to *Boundary Layer Meteorology*.

[3] Jackson P.S. and J.C.R Hunt, 1975: 'Turbulent wind flow over a hill'. *Quart. J. Meteorol. Soc.*, **101**, 929 - 955.

[4] Newley T.J., 1985: 'Turbulent air flow over hills'. PhD Dissertation, University of Cambridge.

[5] Wood N. and P.J. Mason, 1993: 'The pressure force induced by neutral, turbulent flow over hills'. *Quart. J. Meteorol. Soc.*, **119**, 1233 - 1267.